ADVANCED ENERGY MATERIALS
www.advenergymat.de

A Novel Aluminum–Graphite Dual-Ion Battery

Xiaolong Zhang, Yongbing Tang, Fan Zhang, and Chun-Sing Lee**

Lithium ion batteries based on cation intercalation have been powering the increasingly mobile society for decades.[1] In a conventional lithium ion battery, the intercalation of lithium ions in both cathode (i.e., $LiCoO_2$, $LiFePO_4$) and anode (i.e., graphite, silicon) materials have been thoroughly studied, while the utilization of the anions in the electrolyte has drawn much less attention.[2] In fact, the phenomenon of anion intercalate into graphite by chemical or electrochemical means was discovered and proposed as a possible positive electrode for batteries by Rüdorff and Hofmann in 1938.[3] However, the anion intercalation was achieved by using high concentration acid solution as electrolyte, this brought serious safety issue that hindered its application.[4] In the 1990s, soon after the commercial application of lithium ion battery, Carlin et al. reported dual graphite intercalating molten electrolyte batteries that realized the application of anion intercalated graphite as positive electrode in batteries by using room temperature ionic liquids as electrolyte.[5] In the following decades, continuous progresses have been made in anion intercalated graphite based dual carbon batteries, such as investigation of anion intercalation in non-aqueous electrolyte, in situ characterization of the staged anion intercalation process, and systematic study of the intercalation of different anions into graphite.[6] However, due to electrolyte decomposition caused by the high positive potential of anion intercalated graphite (≈5 V vs Li/Li^+) and exfoliation of graphite layers upon repeated ion/solvent molecule intercalation/deintercalation, reported dual-carbon batteries showed unsatisfied charge–discharge reversibility.[7]

A key challenge of developing highly reversible dual-graphite battery is to find a suitable electrolyte enabling both Li^+ intercalation into graphite negative electrode and anion intercalation into graphite positive electrode simultaneously. Conventional carbonate electrolytes were mainly composed of ethylene carbonate (EC), acyclic carbonate, and lithium salt. EC in the electrolyte is an important component for the formation of solid electrolyte interphase (SEI) and the protection of the negative graphitic electrode.[8] Unfortunately, when applied in a dual-graphite battery, the EC molecules in the electrolyte can bind tightly with PF_6^- anions, and prevent the intercalation of these anions into the interlayer spaces of graphite positive electrodes.[9] Recently, with the developments of novel electrolyte formulas, several studies have reported significantly improved reversibility of dual-carbon batteries.[10] Read et al. reported a reversible dual-graphite battery with simultaneous accommodation of Li^+ and PF_6^- in graphitic structures enabled by a high voltage electrolyte based on fluorinated solvent and additive.[10a] The battery demonstrated a reversible capacity of 60 mAh g^{-1} and a capacity retention of 62% after 50 cycles at C/7 rate. Rothermel et al. reported a dual-graphite battery based on a mixture of lithium bis-(trifluoromethanesulfonyl)-imide (LiTFSI) and ionic liquid with SEI-forming additive. This electrolyte formula not only enabled stable $TFSI^-$ intercalation into the graphite positive electrode, but also allowed highly reversible intercalation of Li^+ into the graphite negative electrode.[10b] Under an upper cut-off potential of 5.0 V, the full graphite battery presented a capacity of 97 mAh g^{-1} at a current rate of 10 mA g^{-1}, and 50 mAh g^{-1} at 500 mA g^{-1}, which shed light on the potential application of dual-ion batteries as an environmentally friendly energy storage technology.

Herein, we report a novel aluminum–graphite dual-ion battery (AGDIB) in an ethyl–methyl carbonate (EMC) electrolyte with high reversibility and high energy density. It is the first report on using an aluminum anode in dual-ion battery. The battery shows good reversibility, delivering a capacity of ≈100 mAh g^{-1} and capacity retention of 88% after 200 charge–discharge cycles at 2 C (1 C corresponding to 100 mA g^{-1}). To the best of our knowledge, performance of the battery is among the best of reported dual-ion batteries.

Figure 1a schematically illustrates the initial and charged states of the AGDIB. Upon charging, PF_6^- anions in the electrolyte intercalate into the graphite cathode, while the Li^+ ions in the electrolyte deposit onto the aluminum counter electrode to form an Al–Li alloy. The discharge process is the reverse of the charge process, where both PF_6^- anions and Li^+ ions diffuse back into the electrolyte. The Al counter electrode acts as both the anode and the current collector, which greatly benefits the specific energy density and volumic energy density of the AGDIB.[11] Figure 1b shows galvanostatic charge–discharge curves of the AGDIB, exhibiting a typical profile of anion intercalation/deintercalation into/from graphite. The charge curve is mainly composed of three regions between 4.08 and 4.59 V (stage III), 4.59 and 4.63 V (stage II), and 4.63 and 5.0 V (stage I), each region corresponds to an anion intercalation stage of graphite, according to previous reports.[6e] A dQ/dV differential curve of the battery is shown in the inset of Figure 1b. Peaks in the profile correspond to electrochemical processes in the AGDIB during charge–discharge. Stage III contains three wide weak peaks, while stage II contains a strong peak and small shoulder peak. No obvious peak in stage I can be observed.

X. L. Zhang, Prof. Y. B. Tang, Dr. F. Zhang, Prof. C.-S. Lee
Functional Thin Films Research Center
Shenzhen Institutes of Advanced Technology
Chinese Academy of Sciences
Shenzhen 518055, China
E-mail: tangyb@siat.ac.cn; apcslee@cityu.edu.hk
Prof. C.-S. Lee
On sabbatical leave from the Center
of Super-Diamond and Advanced Film
(COSAD) & Dept. of Phys. & Mater. Sci.
City University of Hong Kong
Hong Kong SAR, China

DOI: 10.1002/aenm.201502588

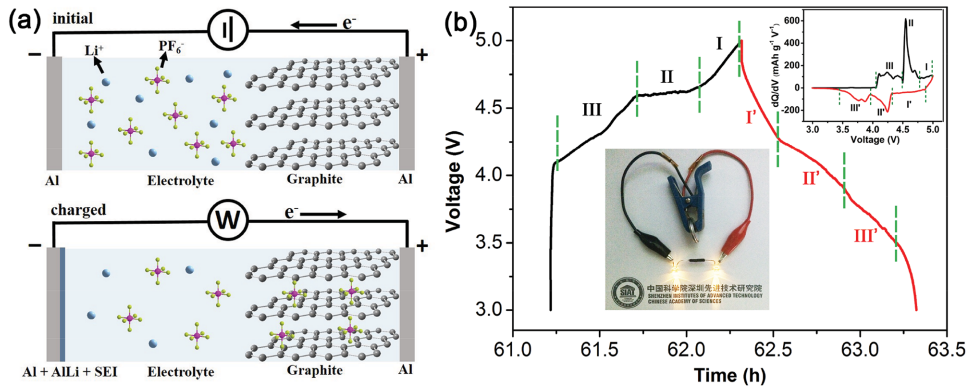

Figure 1. a) Schematic illustration of the AGDIB in the initial state (up) and the charged state (below). b) Galvanostatic charge–discharge curve of the AGDIB at 0.5 C (1 C corresponding to a current rate of 100 mA g^{-1}). Insets are the dQ/dV differential curve of the battery and a photograph showing that a single AGDIB cell lighting up two yellow LEDs in series.

Only three peaks are found in the discharge process, due to the diminish or disappear of two peaks during anion deintercalation process, as reported in previous report.[10b] The AGDIB shows a working voltage range of 4.8–3.4 V with a middle working voltage of ≈4.2 V at 0.5 C current rate, which is much higher than most of those in commercial lithium ion batteries (≈3.7 V).[12] The relative high discharge voltage of the AGDIB enabled a single coin cell to light up two yellow LEDs (nominal voltage of ≈2.5 V) in series (Figure 1b inset).

We believe that the good performance of the AGDIB battery is resulted from its specially designed configuration. Firstly, unlike other reported dual-ion batteries, we use aluminum instead of graphite anode. This design eliminates the needs for an addition metallic current collector and lead to considerable weight saving. Another advantage is that we can now eliminate the use of EC, which is commonly used in the electrolyte for protecting the graphite anode. This allows us to use a 100% EMC solvent in the electrolyte which not only solve the problem of binding between EC and PF_6^-, as reported by Wand and Gao et al.,[9,13] it can also dissolve a much higher concentration of $LiPF_6$ comparing to the commonly used mixed solvents with EC. Seel and Dahn[14] have shown that using a high salt concentration can reduce the potential required for anion intercalation into the graphite cathode. Figure S2 in the Supporting Information shows charge–discharge curves in Li | $LiPF_6$ in EMC | Graphite batteries with different $LiPF_6$ concentrations. As the concentration of $LiPF_6$ increases from 1 to 4 M, the anion intercalation potential decreases from 4.45 to 4.34 V (Figure S2b, Supporting Information). This leads to a corresponding increase in specific capacity from 54 to 84 mAh g^{-1}.

We also found that performance of the battery depends critical on the metal used in the anode. We tested metal | 4 M $LiPF_6$ in EMC | graphite batteries with different metal counter electrodes (Cu, Fe, Li, Al). Surprisingly, the aluminum | 4 M $LiPF_6$ in EMC | graphite battery shows much higher initial discharge capacity and coulombic efficiency than the other batteries (**Figure 2**). As both Cu and Fe are inert to form alloy with lithium, the batteries based on Cu and Fe counter electrodes were unable to maintain the lithium ions deposited on them during the charge process. Therefore, only limited discharge capacities were observed in these batteries. On contrary, aluminum is able to form alloy with lithium and it has been studied as a promising anode material for lithium ion battery.[15] During charge process, lithium ions in the electrolyte obtain electrons on the surface of aluminum counter electrode and form stable aluminum–lithium alloy. This alloy enabled the controlled release of the lithium ions in the discharge process.

Although the Al | 4 M $LiPF_6$ in EMC | Graphite battery exhibits impressive initial discharge capacity, the cycle stability of this battery is poor, resulting from the pulverization caused by the volume expansion of aluminum during the alloying process.[15a] To improve the cycle stability, we tried to add SEI formation additive into the electrolyte to protect the aluminum counter electrode from pulverization. After screening of different electrolyte additives, we found that a small amount of vinylene carbonate (VC) is very effective in improving the cycle stability of the aluminum–graphite battery. Figure S3 in the Supporting Information shows the charge–discharge curves of the formation process of the AGDIB with different amount of VC in the electrolyte. With the presence of VC, the charge curves show an extra plateau at about 4.37 V, which corresponds to the decomposition of VC and the formation of SEI layer.[8b] Meanwhile, the amount of VC was found to be critical for improving the cycle stability of the AGDIB. When the amount of VC is low (i.e., 1 wt%), the battery showed fast capacity decay (Figure S4a, Supporting Information). On the other hand, high amount of VC (i.e., 5 wt%) will lead to relatively lower coulombic efficiency during cycling and a battery failure was tricked after several charge–discharge cycles (Figure S4b, Supporting Information). We found that batteries with 2 wt% VC in the electrolyte showed the best stability. **Figure 3** shows the charge–discharge cycle test results of aluminum–graphite battery with commercial carbonate electrolyte (1 M $LiPF_6$ in EC/EMC/DMC), 4 M $LiPF_6$ in EMC, and 4 M $LiPF_6$ in EMC + 2 wt% VC. With the presence of VC additive, the AGDIB exhibits a reversible discharge capacity of 105 mAh g^{-1} (the seventh cycle) and a capacity retention of 96% after 50 cycles at 0.5 C current rate. For comparison, the capacity of the batteries without VC additive dramatically decayed within the first 20 charge–discharge cycles.

The battery with 2 wt% VC additive was then cycled at various charge–discharge rates ranging from 0.5 to 5 C over a potential window of 3.0–5.0 V. Typical galvanostatic profiles

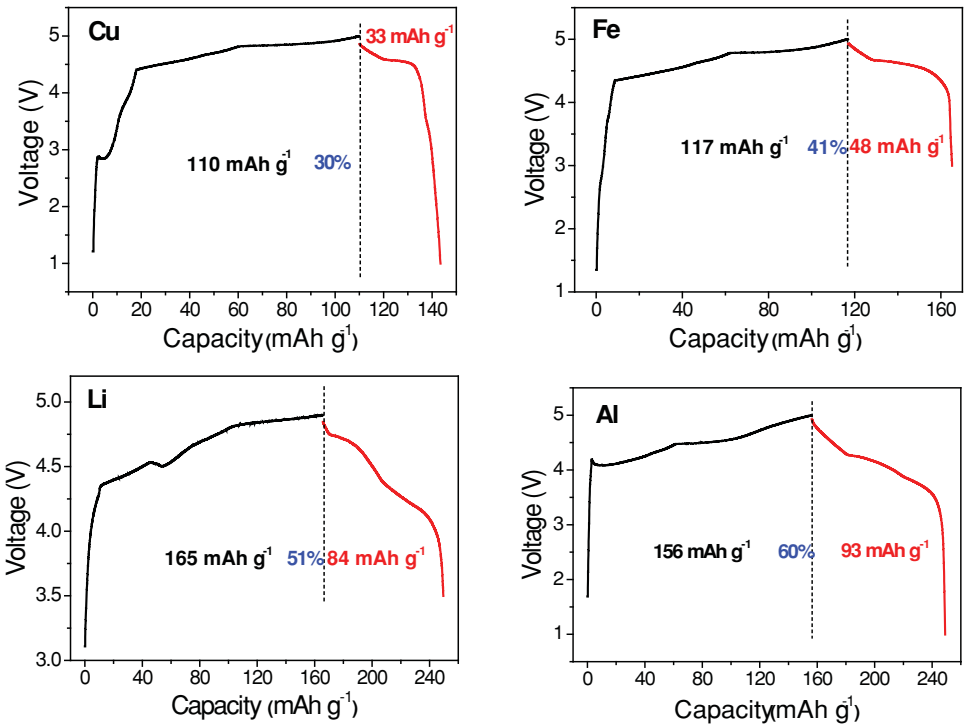

Figure 2. Charge–discharge curves of Metal | 4 M $LiPF_6$ in EMC | Graphite batteries with respectively a) Cu, b) Fe, c) Li, and d) Al counter electrode.

of the battery are shown in **Figure 4**a. All the curves show the typical three-stage charge–discharge profile of anion intercalation in graphite, as discussed before. The gradually increased charge–discharge plateau separation implies small electrode polarization at low current rate and relatively large polarization at high current rates. Figure 4b further shows the charge–discharge capacities and corresponding coulombic efficiencies of the AGDIB during the rate capacity tests. At the rates of 0.5, 1, 2, 3, and 5 C, the battery show discharge capacities of 105, 104, 100, 93, and 79 mAh g^{-1}, respectively. The battery can regain the high capacity when the current rate was set back to lower value gradually, demonstrating its high reversibility. The gradually increasing coulombic efficiencies (67%–83%) during the first few cycles at 0.5 C, was attributed to the formation of protective SEI layer on the surface of the electrodes. After the first 10 cycles at 0.5 C, the battery shows stable coulombic efficiencies at each of the following current rates, with values of 91%, 92%, 96%, and 98% at 1, 2, 3, and 5 C, respectively. Figure 4c illustrates the long term cycling performance of the AGDIB at a current rate of 2 C. Compared with batteries based on anion intercalated graphite reported in literature,[7c,10,16] this AGDIB cell shows much improved cyclability. Notably, the discharge capacity varies from 104 to 92 mAh g^{-1} during the 200 charge–discharge cycles, corresponding to capacity retention of 88% and only 0.06% capacity loss per cycle. The electrochemical performance of this AGDIB is among the best of reported dual-ion batteries (Table S3).

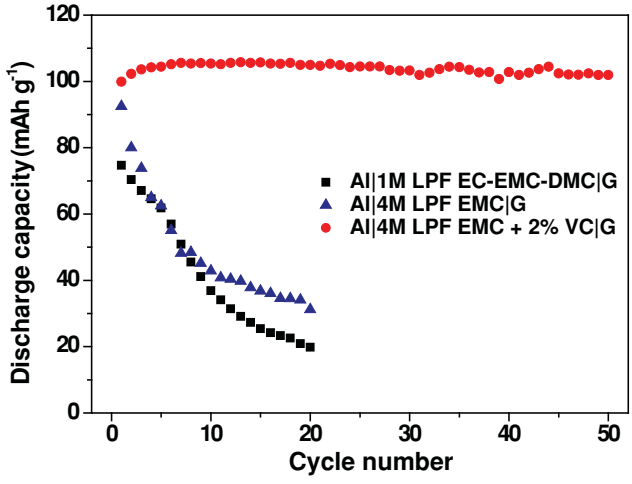

Figure 3. Charge–discharge cycle results of the batteries using different electylotes. The test current rate was 0.5 C. a) Al | 1 M $LiPF_6$ in EC–EMC–DMC | Graphite, b) Al | 4 M $LiPF_6$ in EMC | Graphite, c) Al | 4 M $LiPF_6$ in EMC + 2 wt% VC | Graphite.

The AGDIB reported here was composed of only environmentally friendly low cost materials (i.e., aluminum and graphite) as electrode materials, and conventional lithium salt and carbonate solvent as electrolyte. Compared with conventional secondary battery technologies (mainly lithium ion batteries), it shows an obvious advantage in production cost. Furthermore, as the Al counter electrode in the AGDIB acts as both the anode and the current collector, the dead load and dead volume of this battery could be significantly reduced, which result in a battery with both high specific energy density and high volume energy density. We roughly estimated the specific energy density and power density of the AGDIB based on the tested results and the mass composition of conventional packaged batteries (detail of the calculation is available in supporting materials). The calculation results (Table S1) show that the AGDIB can deliver

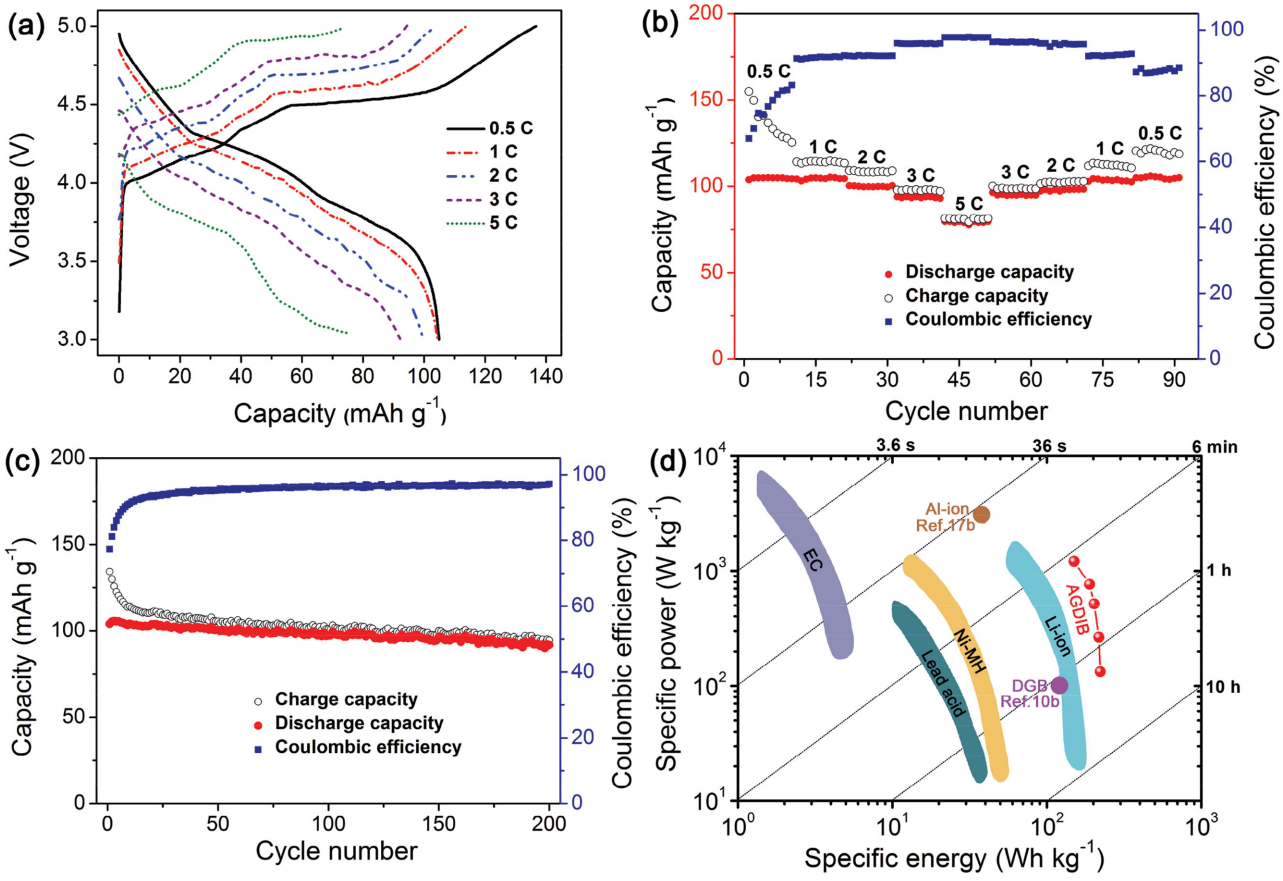

Figure 4. a) Charge–discharge curves of the AGDIB under 0.5, 1, 2, 3, and 5 C current rate (1 C corresponding to 100 mA g^{-1}). b) Rate capacities and corresponding coulombic efficiencies of the AGDIB. c) Long term cycle test result of the AGDIB at a current rate of 2 C. d) Performance comparison of the AGDIB with conventional electrochemical energy storage devices and several recently reported advanced energy storage devices, where DGB represents dual-graphite battery.

a specific energy density of ≈222 Wh kg^{-1} at a power density of 132 W kg^{-1}, and ≈150 Wh kg^{-1} at 1200 W kg^{-1}. Figure 4d shows a comparison of the AGDIB with several main-stream energy storage technologies. Apparently, comparing with commercial lithium ion battery (≈200 Wh kg^{-1} at 50 W kg^{-1}, and ≈100 Wh kg^{-1} at 1000 W kg^{-1}) and electrochemical capacitor (≈5 Wh kg^{-1} at 5000 W kg^{-1}), the AGDIB shows significantly improved performances.[17]

To understand the charge–discharge mechanism of the AGDIB, further characterizations of the electrodes were carried out. The anion intercalation in graphite positive electrode is a reported phenomenon. The intercalation of PF_6^- (size of 4.36 Å)[18] into graphite sheets (distance of 3.36 Å) is accompanied by significant inter space expansion and gradual exfoliation of the graphite sheets (Figure S5, Supporting Information), which is responsible for the slow capacity degradation during cycling. The electrochemical process on the Al counter electrode is of great interests. The charge–discharge curves of a Li–Al half cell is shown in Figure S6 in the Supporting Information. It shows that the Al–Li alloying process on the aluminum electrode exhibited a flat plateau at about 0.22 V versus Li/Li^+, and 0.52 V versus Li/Li^+ during dealloying process. **Figure 5**a,b shows photographs of the Al electrodes before and after charged in the AGDIB. A rough layer on the surface of the charged Al electrode could be observed by naked eyes. Scanning electron microscopic (SEM) image shows that the rough layer possess nanoporous microstructures (Figure 5d), which was likely to be caused by the formation of SEI layer and the Al–Li alloying process. Energy dispersive X-ray spectroscopy (EDS) mapping (Figure S7 and Table S2, Supporting Information) on the surface of the charged Al electrode show the existence of F, C, and O, which are common composing elements of SEI layers.[19] This SEI layer could protect the Al electrode from destruction during Li–Al alloying and dealloying process. For comparison, much less elements component of SEI layer were found (Figure S8, Supporting Information) on the surface of Al electrode without the presence of VC. Without the protection of SEI layer, pulverization and cracks were found on the surface of the Al electrode (Figure S9, Supporting Information).The existence of Al–Li alloy on the charged Al electrode was verified by the XRD patterns (Figure 5e), where diffraction peaks of both Al (JCPDS Card No. 65-2869) and AlLi (JCPDS Card No. 65-3017) can be clearly observed. According to the characterization results, electrochemical reactions in the AGDIB are proposed as follows.

The half cell reaction at the negative electrode is considered to be

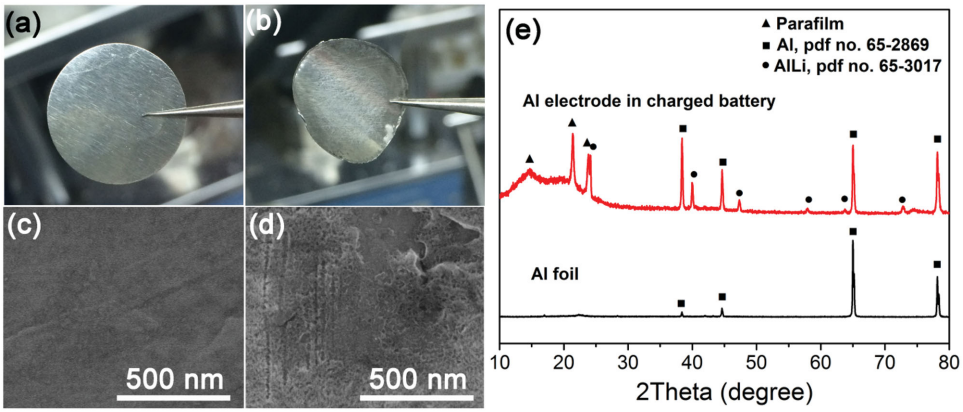

Figure 5. Photographs of a) a fresh Al foil and b) an Al electrode in a charged battery. SEM images of c) a fresh Al foil and d) an Al electrode in a charged battery. e) XRD patterns of a fresh Al foil (below) and an Al electrode in a charged battery (up).

$$Al + Li^+ + e^- \leftrightarrow AlLi \quad (1)$$

And the half cell reaction at the positive electrode is considered to be[14]

$$xC + PF_6^- \leftrightarrow C_x(PF_6) + e^- \quad (2)$$

The full cell reaction is

$$Al + xC + Li^+ + PF6^- \leftrightarrow AlLi + C_x(PF_6) \quad (3)$$

The Al–Li alloying process has been studied as a potential anode of lithium ion battery in previous works.[15,20] The theoretical capacity of aluminum could reach 2235 mAh g^{-1} in the form of Li_9Al_4. However, the lithiation of aluminum faces a ≈100% volume expansion, which would tear up the anode SEI layer and cause the pulverization of the active material. Here in the AGDIB, the lithiation of Al electrode was stabilized for the following two reasons. Firstly, compared with the deep lithiation in Li_9Al_4, the volume expansion caused by the shallow lithiation (AlLi) in the present AGDIB is smaller, which could help reduce the stress in the Al electrode caused by lithiation. Secondly, VC induced SEI layer on the surface of Al electrode could protect the Al electrode from destruction caused by the Li–Al alloying process. Detailed mechanism of this AGDIB battery, in particularly the role of VC are still under further investigation.

In summary, we have developed a novel AGDIB composed of only environmentally friendly low-cost materials (i.e., aluminum as counter electrode, graphite as positive electrode), and a specially designed carbonate electrolyte. As aluminum acted as both the negative current collector and the negative active material, the AGDIB shows significantly reduced dead load and dead volume. The AGDIB delivers a reversible capacity of 104 mAh g^{-1} (based on the mass of graphite) at 2 C current rate, and a capacity retention of 88% after 200 cycles. According to the composition of conventional packaged battery, a packaged AGDIB cell is estimated to delivery an energy density of ≈220 Wh kg^{-1} at a power density of ≈130 W kg^{-1}, and ≈150 Wh kg^{-1} at ≈1200 W kg^{-1}, which are significantly higher than most commercial lithium ion batteries, indicating its potential to be a low-cost power source with both high energy density and high power density.

Experimental Section

Aluminum foil (thickness of 15 μm) purchased from Shenzhen Kejingstar was used as the counter electrode. The graphite positive electrode composes of 80 wt% of natural graphite (d_{002} spacing of 3.363 Å, SEM image shown in Figure S1, Supporting Information), 10 wt% of conductive carbon black, and 10 wt% of polyvinylidene fluoride (PVDF) as binder.*N*-methyl-2-pyrrolidone (NMP) was added to the above mixture and grounded to form a uniform slurry. Then the slurry was pasted onto aluminum foil and dried in vacuum in an 80 °C oven. The mass loading of the graphite positive electrode was 1.5 mg cm^{-2}.The components of the electrolyte, namely EMC, VC, and $LiPF_6$ were used as purchased from Dodochem. The commercial electrolyte, 1 M $LiPF_6$ EC–EMC–DMC (1:1:1), was kindly provided by Capchem.

Powder X-ray diffraction (XRD) analysis was carried out on a Rigaku D/Max-2500 diffractometer using Cu Kα radiation with a scan rate of 8° min^{-1}, operating at 40 kV and 30 mA. XRD samples of the charged electrodes were prepared in glove box, washed with EMC, and coated with parafilm to protect them from been oxidized by air. SEM images were collected on a HITACHI S-4800 field emission scanning electron microscope.

Electrochemical tests were performed with CR2032 coin-type cells. The graphite positive electrode was countered with different metal electrodes (Li, Al, Fe, Cu). Lab-made electrolyte or the purchased commercial electrolyte were used as the electrolyte and glass fiber was used as separator. The preparation of electrolyte and fabrication of battery were conducted in an argon filled glove box (Etelux Lab2000). Cyclic voltammetry (CV) tests were done on an AUTOLAB PGSTAT302N electrochemical station. Galvanostatic charge–discharge tests were carried out on LAND CT2011A battery test system at room temperature.

Supporting Information

Supporting Information is available from the Wiley Online Library or from the author.

Acknowledgements

This project was financially supported by the National Natural Science Foundation of China (Nos. 51272217, 51302238), Science and Technology Planning Project of Guangdong Province (Nos. 2014A010105032, 2014A010106016), Guangdong Innovative and Entrepreneurial Research Team Program (No. 2013C090), Shenzhen Municipality Project (No. JCYJ20140417113430618, JSGG20150602143328010), and Scientific Equipment Project of Chinese Academy of Sciences (yz201440)

Received: December 31, 2015
Revised: January 28, 2016
Published online: March 15, 2016

[1] a) D. Larcher, J. M. Tarascon, *Nat. Chem.* **2015**, *7*, 19; b) J. B. Goodenough, K. S. Park, *J. Am. Chem. Soc.* **2013**, *135*, 1167; c) J. Cabana, L. Monconduit, D. Larcher, M. R. Palacín, *Adv. Mater.* **2010**, *22*, E170.
[2] A. Vlad, N. Singh, C. Galande, P. M. Ajayan, *Adv. Energy Mater.* **2015**, *5*, 1402115.
[3] W. Rüdorff, U. Hofmann, *Z. Anorg. Allg. Chem.* **1938**, *238*, 1.
[4] F. Beck, H. Junge, H. Krohn, *Electrochim. Acta* **1981**, *26*, 799.
[5] R. T. Carlin, H. C. De Long, J. Fuller, P. C. Trulove, *J. Electrochem. Soc.* **1994**, *141*, L73.
[6] a) T. Placke, S. Rothermel, O. Fromm, P. Meister, S. F. Lux, J. Huesker, H. W. Meyer, M. Winter, *J. Electrochem. Soc.* **2013**, *160*, A1979; b) T. Ishihara, Y. Yokoyama, F. Kozono, H. Hayashi, *J. Power Sources* **2011**, *196*, 6956; c) T. E. Sutto, T. T. Duncan, T. C. Wong, *Electrochim. Acta* **2009**, *54*, 5648; d) W. C. West, J. F. Whitacre, N. Leifer, S. Greenbaum, M. Smart, R. Bugga, M. Blanco, S. R. Narayanan, *J. Electrochem. Soc.* **2007**, *154*, A929; e) M. Noel, R. Santhanam, *J. Power Sources* **1998**, *72*, 53.
[7] a) J. Gao, M. Yoshio, L. Qi, H. Wang, *J. Power Sources* **2015**, *278*, 452; b) X. Qi, B. Blizanac, A. DuPasquier, P. Meister, T. Placke, M. Oljaca, J. Li, M. Winter, *Phys. Chem. Chem. Phys.* **2014**, *16*, 25306; c) H. Nakano, Y. Sugiyama, T. Morishita, M. J. S. Spencer, I. K. Snook, Y. Kumai, H. Okamoto, *J. Mater. Chem. A* **2014**, *2*, 7588.
[8] a) J. Li, C. Ma, M. Chi, C. Liang, N. J. Dudney, *Adv. Energy Mater.* **2015**, *5*, 1401408; b) K. Xu, *Chem. Rev.* **2014**, *114*, 11503.
[9] H. Wang, M. Yoshio, *Chem. Commun.* **2010**, *46*, 1544.
[10] a) J. A. Read, A. V. Cresce, M. H. Ervin, K. Xu, *Energy Environ. Sci.* **2014**, *7*, 617; b) S. Rothermel, P. Meister, G. Schmuelling, O. Fromm, H.-W. Meyer, S. Nowak, M. Winter, T. Placke, *Energy Environ. Sci.* **2014**, *7*, 3412.
[11] a) V. Aravindan, Y. S. Lee, S. Madhavi, *Adv. Energy Mater.* **2015**, *5*, 1402225; b) Z. Cai, L. Xu, M. Yan, C. Han, L. He, K. M. Hercule, C. Niu, Z. Yuan, W. Xu, L. Qu, K. Zhao, L. Mai, *Nano Lett.* **2015**, *15*, 738.
[12] a) X. Zhang, F. Cheng, J. Yang, J. Chen, *Nano Lett.* **2013**, *13*, 2822; b) A. Kraytsberg, Y. Ein-Eli, *Adv. Energy Mater.* **2012**, *2*, 922.
[13] J. Gao, S. Tian, L. Qi, M. Yoshio, H. Wang, *J. Power Sources* **2015**, *297*, 121.
[14] J. A. Seel, J. R. Dahn, *J. Electrochem. Soc.* **2000**, *147*, 892.
[15] a) S. Li, J. Niu, Y. C. Zhao, K. P. So, C. Wang, C. A. Wang, J. Li, *Nat. Commun.* **2015**, 6; b) J. H. Park, C. Hudaya, A. Y. Kim, D. K. Rhee, S. J. Yeo, W. Choi, P. J. Yoo, J. K. Lee, *Chem. Commun.* **2014**, *50*, 2837; c) E. C. Gay, D. R. Vissers, F. J. Martino, K. E. Anderson, *J. Electrochem. Soc.* **1976**, *123*, 1591.
[16] a) M. L. Aubrey, J. R. Long, *J. Am. Chem. Soc.* **2015**; b) P. Meister, V. Siozios, J. Reiter, S. Klamor, S. Rothermel, O. Fromm, H.-W. Meyer, M. Winter, T. Placke, *Electrochim. Acta* **2014**, *130*, 625; c) G. Park, N. Gunawardhana, C. Lee, S. M. Lee, Y. S. Lee, M. Yoshio, *J. Power Sources* **2013**, *236*, 145; d) A. K. Thapa, G. Park, H. Nakamura, T. Ishihara, N. Moriyama, T. Kawamura, H. Y. Wang, M. Yoshio, *Electrochim. Acta* **2010**, *55*, 7305.
[17] a) T. Lin, I.-W. Chen, F. Liu, C. Yang, H. Bi, F. Xu, F. Huang, *Science* **2015**, *350*, 1508; b) M. C. Lin, M. Gong, B. Lu, Y. Wu, D. Y. Wang, M. Guan, M. Angell, C. Chen, J. Yang, B. J. Hwang, H. Dai, *Nature* **2015**, *520*, 325; c) F. Zhang, T. Zhang, X. Yang, L. Zhang, K. Leng, Y. Huang, Y. Chen, *Energy Environ. Sci.* **2013**, *6*, 1623; d) T.-H. Kim, J.-S. Park, S. K. Chang, S. Choi, J. H. Ryu, H.-K. Song, *Adv. Energy Mater.* **2012**, *2*, 860; e) A. Du Pasquier, I. Plitz, S. Menocal, G. Amatucci, *J. Power Sources* **2003**, *115*, 171.
[18] J. A. Read, *J. Phys. Chem. C* **2015**, *119*, 8438.
[19] K. Tasaki, A. Goldberg, J.-J. Lian, M. Walker, A. Timmons, S. J. Harris, *J. Electrochem. Soc.* **2009**, *156*, A1019.
[20] C. J. Wen, B. A. Boukamp, R. A. Huggins, W. Weppner, *J. Electrochem. Soc.* **1979**, *126*, 2258.